applied sciences

MDPI

Article

Enhancing Friction Pendulum Isolation Systems Using Passive and Semi-Active Dampers

Christian A. Barrera-Vargas [1], Iván M. Díaz [1,*], José M. Soria [1] and Jaime H. García-Palacios [2]

[1] Department of Continuum Mechanics and Theory of Structures, ETS Ingenieros Caminos, Canales y Puertos, Universidad Politécnica de Madrid, 28040 Madrid, Spain; christian.barrera.vargas@alumnos.upm.es (C.A.B.-V.); jm.soria@upm.es (J.M.S.)

[2] Department of Hydraulics, Energy and Environmental Engineering, ETS Ingenieros Caminos, Canales y Puertos, Universidad Politécnica de Madrid, 28040 Madrid, Spain; jaime.garcia.palacios@upm.es

* Correspondence: ivan.munoz@upm.es

Received: 4 July 2020 ; Accepted: 10 August 2020; Published: 13 August 2020

Abstract: Friction pendulum systems (FPSs) are a common solution for isolating civil engineering structures under ground movements. The result is a base-isolated structure in which the base exhibits low shear stiffness in such a way that the input energy of the earthquake is concentrated and dissipated into it, leaving the superstructure free of damage. As a consequence, large displacements of the FPS may be demanded depending on the earthquake intensity and the fundamental period of the FPS. To accommodate these displacements, large-size isolators with high friction coefficients are usually required. However, the FPS will then exhibit poor re-centering capacity and the risk of future shocks will increase due to previous residual displacements, especially for low-intensity earthquakes. An alternative solution is to include a semi-active damper to the FPS, keeping the friction coefficient low and achieving both, limited base displacement under high-intensity earthquakes and good re-centering capacity under low-intensity ones. Thus, this work presents a design methodology for base isolators formed by an FPS with a damper added. The design methodology is applied to an FPS with a passive damper and to an FPS with a semi-active damper. Two ON-OFF control strategies are studied: (i) a fairly simple phase control, and (ii), a mechanical energy-predictive based algorithm. The advantages of semi-active FPSs with low friction coefficients with respect to FPS with high friction coefficients are demonstrated. The results with the designed semi-active FPS are compared with the single FPS and the FPS with a passive damper. Finally, the use of semi-active FPS allows us to enhance the FPS performance as the isolator size can be reduced while keeping the capacity to cope with low and high-intensity earthquakes without residual displacements.

Keywords: base isolation; friction pendulum system; semi-active control; phase control; energy-predictive-based control

1. Introduction

Base isolation systems are implemented to mitigate the damage and minimize the risk of collapse of structures due to earthquake vibrations. The base is designed to exhibit low shear stiffness and to be able to cope with large displacement in such a way that the input energy is concentrated and dissipated into it [1,2]. Thus, the isolators are usually designed to move the first-mode period of the structure out of the maximum acceleration of the design response spectrum through a higher fundamental period of the isolator system. This concept has given satisfactory results, allowing the development of different types of isolators, with linear and/or nonlinear behavior such as lead-rubber bearings, high damping rubber bearings, and friction pendulum systems (FPSs), these being the most common ones [3]. However, due to the uncertain nature of the earthquakes, the behavior of these passive

isolation devices may not be as desirable as expected. That is, if the frequency content of the excitation is significantly greater than the fundamental frequency of the base-isolated structure, the ground movement will be effectively filtered out. On the contrary, if the excitation shows frequency content in the vicinity of the fundamental frequency, large undesirable oscillations may take place.

The FPS allows us to unlink the foundation from the structure and to dissipate energy from the earthquake through its displacement. Greater dissipation on the device is achieved when large isolator displacements are allowed. The isolator displacements will initially depend on the dry friction, then, the displacement will be governed by the pendulum stiffness directly related to the concave plate radius of curvature and the dynamic friction. The later may affect the existence of residual displacements after the seismic event [4].

Three generations of FPSs have been studied until now. The first generation consists of two plates, where one of them has a concave surface, and the second plate (bearing plate) slides over the first one. The bearing displacements are limited by the concave plate-size. The second generation is characterized by having both concave surfaces, obtaining double friction capacity, double stiffness and more bearing displacement capacity [5]. The third generation is a compound of two isolators of the type of the second-generation, one inside the other. This generation develops more bearing displacement capacity, that is, allows the dissipating of more energy as compared to the second generation by having the double of concave surfaces [6]. Figure 1 illustrates these generations.

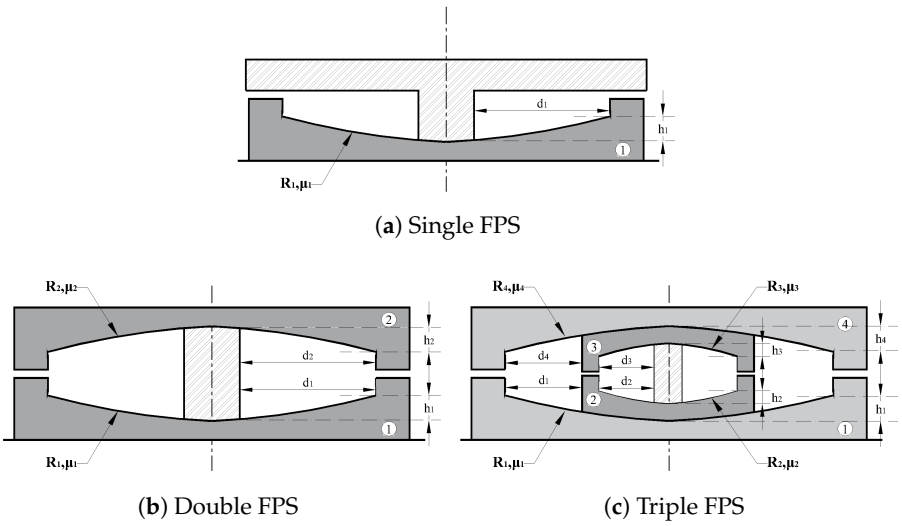

Figure 1. Variations of friction pendulum systems, R is the concave plate radius and μ is the dynamic friction coefficient.

Much research has been done on the analysis of the FPS performance and its design. Some studies are focused on investigating the different variables that affect the behavior of FPSs, such as the influence of the FPS temperature when it is working, or the performance of FPSs under bidirectional effects [7]. Others studies are mainly focused on simplified methodologies that allow designers to analyze isolated-structures with FPSs [8]. Most of the design methodologies focus on finding the optimal pendulum geometry by minimizing the peak acceleration of the structure [9,10]. Generally, to achieve lower structural accelerations, higher displacement demands of the FPS will have to be accommodated. Thus, a larger size isolator will be required. To reduce the isolator displacement demand, and consequently the isolator size, devices with a higher friction coefficient may be used. Although the displacement demand is reduced, the re-centering capacity is drastically affected [4]. That is, under low-intensity earthquakes, residual displacements may take place, increasing thus the risk for future shocks [11]. Additionally, high friction FPSs may show problems related to the pre-sliding phase; that is, the FPS may not be engaged even for a moderate earthquake. Therefore, an FPS with low-friction damping (i.e., with good re-centering capacity) and with increased stiffness

at large displacement is desirable. To achieve this objective, the addition of a smart damper becomes a possible solution.

Several studies about hybrid seismic isolation systems, which use passive isolation devices and smart devices, such as, actively controlled actuators [12,13] or magnetorheological (MR) dampers working as a semi-active control strategy [14–16], have been developed. The main goal of using a hybrid isolation system is to limit the large base-displacement demand on the passive isolator without affecting the benefits obtained in the reduction of the acceleration or inter-story drift of the structure. To achieve this improvement, an appropriate control law that governs the response of the active or semi-active damper must be defined, otherwise, the effect on the structure may become undesirable and even unstable in the case of active isolation. Koo et al. [17] studied some control laws for the design of semi-active tuned vibration absorbers (TVAs) using the groundhook concept, in which the groundhook simulates a "hook" between the structure to be controlled and the "ground", where the ground is the base support perturbated (e.g., a building foundation). Weber et al. [18] have studied a control law for a single FPS with a semi-active damper, where the semi-active damper response is based on the bearings plate displacement and tries to produce zero dynamic stiffness in the system. Zhang et al. [19] have recently presented an optimum control algorithm that combines a linear quadratic regulator and a nonlinear robust compensator. That is, the proposed control is model-based and is a compound of a state-space feedback and a non-linear compensator to account for isolator nonlinearities. Gu et al. [20] have proposed a "Smart" base isolation, based on using MR elastomers. This isolation system uses an optimal neuro-fuzzy logic control as a control strategy, which intends to control the structure acceleration and the base displacement, simultaneously. Other investigations are focused on full-scale experimental tests of smart-isolated structures. Spencer and Dyke [21] presented an experimental test to prove the effectiveness of an MR damper use as semi-active seismic response control. The control law used in this experiment corresponds to acceleration feedback. Fu et al. [22] have carried out an experimental investigation of a hybrid isolation system which consists in a rubber bearings and an MR damper. The high-order single step control algorithm with an ON-OFF control was used. This method needs to estimate the whole system state in order to compute the optimal control force. Generally, simple control strategies based on feedbacking magnitudes that can be easily measured and/or reliably estimated are always preferred. Additionally, collocated control strategies are also preferred for stability reasons [23].

This paper presents a two-step design methodology for an FPS with a passive or semi-active damper. For the semi-active version, two ON-OFF control laws are studied in depth. The first control law is a fairly simple phase control adapted from the groundhook concept presented by Koo et al. [17] for semi-active TVAs. The second control law is adapted from the energy-predictive algorithm presented by Zelleke [24] to control the magnitude of the mechanical energy in structures with TVAs and it is applied to the problem of the semi-active isolation. The methodology proposed herein accounts for low and high-intensity earthquakes and minimizes a performance function that considers a balance between peak and root-mean-square (RMS) values (accounting for the duration of the event) of several representative performance indexes: structure acceleration, bearing plate displacement and inter-story drift. Additionally, the mechanical energy of the isolated structure is also assessed. Each performance index (PI) is included in the performance function with a particular weighting factor. So, different configurations of weighting factors have been studied and a final configuration that gives priority to the reduction of the inter-story drift of the structure has been finally chosen.

The paper continues with a description of the isolation system and the control laws. The input ground acceleration, a sensitivity analysis for the PIs and the proposed optimization problem are described in Section 3. The results for different configurations of the isolation system are presented and compared in Section 4. In Section 5, the performance of the different configurations is studied under a number of selected earthquakes. Additionally, the performance of the different configurations for a range of concave plate radii, for the same concave plate radius and for a range of friction coefficients

are studied and discussed. Finally, some concluding remarks and suggestions for future work are given in Section 6.

2. Isolation System

The passive version of the FPS is described in Section 2.1. In Section 2.2, a semi-active FPS achieved via a controlled smart damper is presented. Then, two semi-active laws (Sections 2.3 and 2.4) are depicted.

2.1. Friction Pendulum System

The FPS consists of a concave plate slider, over which the main structure can slide during the earthquake (see Figure 2a). The design of the isolator depends mainly on its geometry and on the frictional coefficient of the material. Figure 2b describes the hysteretic behavior of this type of isolators. The fundamental period of the FPS is:

$$T = 2\pi \cdot \sqrt{\frac{R}{g}}, \tag{1}$$

in which R is the radius of the pendulum and g the acceleration of gravity, and the equation that describes the hysteretic behaviour of an FPS is given by:

$$F = k_a \cdot x \pm F_f \quad \text{with} \quad ka = \frac{W}{R_{eff}}, \tag{2}$$

the first term represents the restoring force and the second one is the friction force. The isolator restoring stiffness k_a is obtained from the weight of the structure, W, over the bearing plate of the FPS, and the effective radius, R_{eff}, defined as the concave plate radius minus its height from the inner edge (Figure 2a). The variables x, $\dot{x}$ are the displacement and the velocity of the plate caused by the earthquake, with a maximum value equal to d_1 (displacement capacity). The friction force F_f has two phases: *pre-sliding* and *sliding*, which are modelled as follows:

$$F_f = \begin{cases} k_h x & \text{Pre-sliding} \\ sign(\dot{x})\mu W & \text{Sliding} \end{cases}, \tag{3}$$

in which the *pre-sliding* phase is characterized by a very high initial stiffness (k_h), typically k_h is chosen to be of two orders of magnitude greater than the restoring stiffness k_a and μ is the dynamic friction coefficient which will be assumed constant within the design methodology. For high values of μ, the pre-sliding phase and the so-called breakaway effects are of great importance in case of low-intensity (serviceability) earthquakes. High values of μ could impede the re-centering of the FPS once the earthquake has ended, generating undesirable residual displacements [4,11].

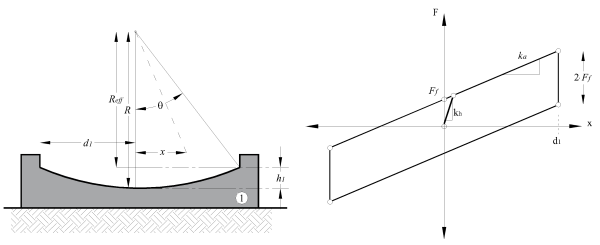

(**a**) Geometric parameters (**b**) Hysteretic diagram

Figure 2. Concave plate geometry and simplified hysteretic diagram. R: Radius of the isolator. h_1: height from the inner edge of the plate. R_{eff}: Effective radius ($R - h_1$). d_1: Displacement capacity.

2.2. Semi-Active FPS

A single-degree-of-freedom model of a structure with an isolator system formed by an FPS and a viscous damper is adopted as shown Figure 3, in which m_p, c_p and k_p are the mass, damping coefficient and stiffness of the structure, x_p and x_a are the structure and bearing plate displacement relative to the base movement and $\ddot{x}_g$ is the ground acceleration. Thus, the study carried out in this paper will consider three models: (i) the structure with an FPS modelled by k_a, F_f (Equations (2) and (3)) and a bearing plate mass, m_a, (ii) the structure with an FPS and a viscous damper with a damping coefficient c_a, denoted as FPS+VD, and (iii) the structure with an FPS and a time-varying damping coefficient which is updated following a particular semi-active control law, denoted as FPS+SD. Figure 4 illustrates these aforementioned cases.

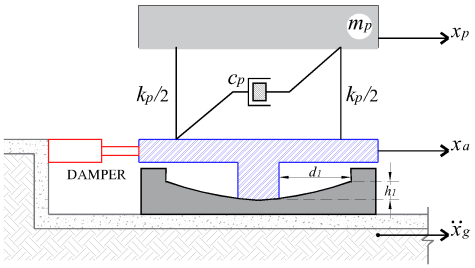

Figure 3. Schematic model of an isolated-structure with a friction pendulum system (FPS) and a damper.

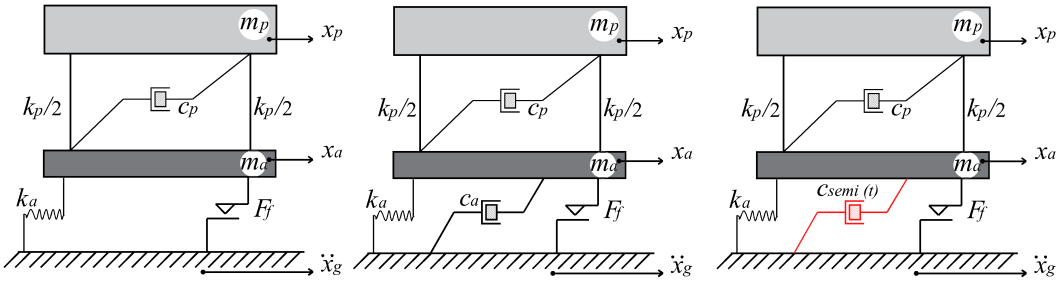

(**a**) FPS (**b**) FPS+VD (**c**) FPS+SD

Figure 4. Considered Models.

The equation of motion of a structure modeled as a single-degree-of-freedom system subjected to a base movement is:

$$m_p\ddot{x}_p + c_p(\dot{x}_p - \dot{x}_a) + k_p(x_p - x_a) = -m_p\ddot{x}_g, \tag{4}$$

where " $\dot{}$ " and " $\ddot{}$ " indicates velocity and acceleration, respectively. Note that Equation (4) is the same for the three cases presented in Figure 4.

The equation of motion of the bearing plate considering a mass of m_a is now derived for the three cases. For the case of a single FPS isolator, this equation is as follows:

$$m_a\ddot{x}_a + F_f(sign(\dot{x}_a)) + k_a x_a - c_p(\dot{x}_p - \dot{x}_a) - k_p(x_p - x_a) = -m_a\ddot{x}_g, \tag{5}$$

for the FPS+VD is:

$$m_a\ddot{x}_a + c_a\dot{x}_a + F_f(sign(\dot{x}_a)) + k_a x_a - c_p(\dot{x}_p - \dot{x}_a) - k_p(x_p - x_a) = -m_a\ddot{x}_g, \tag{6}$$

in which c_a is a fixed damping coefficient of the viscous damper, and finally, for the FPS+SD, the equation takes the following form:

$$m_a\ddot{x}_a + c_{semi}\dot{x}_a + F_f(sign(\dot{x}_a)) + k_a x_a - c_p(\dot{x}_p - \dot{x}_a) - k_p(x_p - x_a) = -m_a\ddot{x}_g, \quad (7)$$

in which $c_{semi}(t)$ is updated continuously following a control law. Two semi-active control laws are proposed to be studied in this paper: phase control and energy-predictive-based control law.

2.3. Phase Control Law

The semi-active control law proposed by Koo et al. [17] for semi-active TVAs has been reformulated to semi-active vibration isolation. More concretely, the concept of the displacement-based groundhook control law has been applied to the relative movement between the ground and the bearing plate. Figure 5 illustrates the phase control logic.

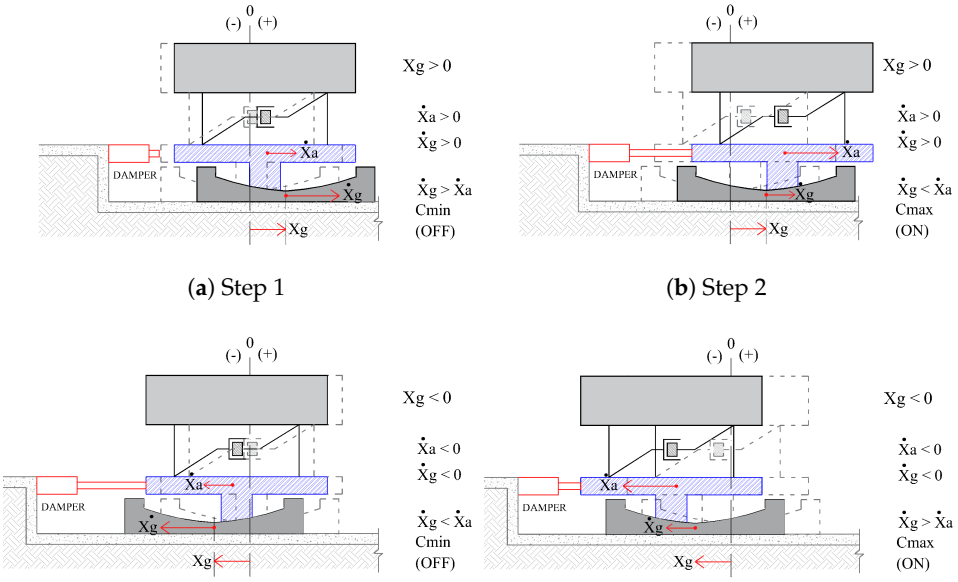

(**a**) Step 1 (**b**) Step 2

(**c**) Step 3 (**d**) Step 4

Figure 5. Illustrations of the phase control logic.

Basically, according to the ground displacement (or the concave plate displacement) and the relative velocity between the ground and the bearing plate, when both are separating, the damper force should pull the structure to the equilibrium point (ON), and, when both are coming together, the damper force should leave the structure free to reach to the equilibrium point (OFF). Thus, the following phase control law assuming absolute magnitudes is derived:

$$\begin{array}{lll} x_g \cdot (\dot{x}_g - \dot{x}_a) \geq 0 & \Rightarrow & c_{min} \quad \text{(normal functioning)} \\ x_g \cdot (\dot{x}_g - \dot{x}_a) < 0 & \Rightarrow & c_{max} \quad \text{(blocking functioning)} \end{array}', \quad (8)$$

in which c_{min} indicates normal functioning and the control law is disabled, and c_{max} indicates blocking functioning and the control law maximize the damper force.

The groundhook-based phase control can be modified by substituting ground displacement by ground acceleration and changing the sign of Inequation (8). Furthermore, since relative magnitudes to the base movement are assumed (Equations (4)–(7)), the phase control law adopted in this work is as follows:

$$\begin{array}{lll} \ddot{x}_g \cdot (\dot{x}_a) \geq 0 & \Rightarrow & c_{min} \quad \text{(normal functioning)} \\ \ddot{x}_g \cdot (\dot{x}_a) < 0 & \Rightarrow & c_{max} \quad \text{(blocking functioning)} \end{array}. \quad (9)$$

Note that this control law is fairly simple and clearly geared to practical implementation due to the measured real-time magnitudes: the concave plate acceleration (instead of its displacement) and the bearing plate velocity.

2.4. Energy-Predictive-Based Control Law

Zelleke and Matsagar [24] have recently presented an energy-predictive-based control law applied to semi-active TVAs. Taking as the main assumption that the ground acceleration remains constant for a time interval (sampling time), the energy is computed for both c_{min} and c_{max}. Thus, the estimation of mechanical energy, which is usually known in the energy-based design methodology as the elastic vibrational energy [2], is derived. Hence, the prediction which produces the minimum mechanical energy provides the desirable damping for the time interval considered. This assumption is mathematically expressed as:

$$\ddot{x}_g(t + \Delta t) = \ddot{x}_g(t), \tag{10}$$

with Δt being the sampling time and t indicates a time instant. Thus, under this assumption, the mechanical energy estimated at the next time instant is:

$$\check{E}_m(t + \Delta t) = \check{E}_k(t + \Delta t) + \check{E}_e(t + \Delta t), \tag{11}$$

in which E_m, E_k, and E_e are the mechanical, kinetic, and elastic strain energy, respectively, and " ˇ " indicates that it is an estimated value. So, the control law can be defined as:

$$\begin{array}{lcll} \check{E}_m(t + \Delta t, c_{min}) < \check{E}_m(t + \Delta t, c_{max}) & \Rightarrow & c_{min} & \text{(normal functioning)} \\ \check{E}_m(t + \Delta t, c_{min}) > \check{E}_m(t + \Delta t, c_{max}) & \Rightarrow & c_{max} & \text{(blocking functioning)} \end{array}. \tag{12}$$

Some remarks about this control law are: (i) contrary to the phase control, the global isolated-structure behavior is considered, (ii) the implementation requires to measure the movement of all the degrees of freedom, (iii) the displacement needed for the computation of elastic energy is difficult to be measured experimentally, (iv) since this is a model-based control law, a real-time response accurate model is needed and consequently, the computational burden will be a critical issue, and finally, (v) the energy computation may include the isolator energy or not.

3. Isolator Design

The proposed methodology for the design of the isolator is presented hereafter. It consists of a two-step design process that makes use of two different excitations (serviceability and design earthquake), which are firstly described in Section 3.1. Secondly, different PIs are defined for both their use within the design process and comparison between design cases. Thirdly, a sensitivity analysis is undergone in Section 3.3 in order to motivate the design process presented in Section 3.4.

3.1. Excitation

To carry out the design of the isolator, two excitations are considered taking into account the different requirements depending on the level of the ground motion: (i) low-intensity ground motion, denoted as serviceability earthquake and (ii) design earthquake for a particular seismic zone. Several synthetic artificial accelerograms are generated from a design spectrum (which is taken here from the Maximum Considered Earthquake (MCE) as it is defined in code ASCE 7-16 [1]).

3.1.1. Serviceability Earthquake

The excitation signal considered for low-intensity ground motion corresponds to earthquakes of intensity less or equal to type VI, with a magnitude from 5.0 < Mw < 5.6 and acceleration (g) between 0.06 to 0.07, characterized by causing minor damages and a maximum of 120 earthquakes per year. Thus, the Livermore earthquake of magnitude Mw = 5.5, that shocked the San Francisco Bay in January 1980, have been used here. Figure 6 shows the input ground acceleration of this earthquake.

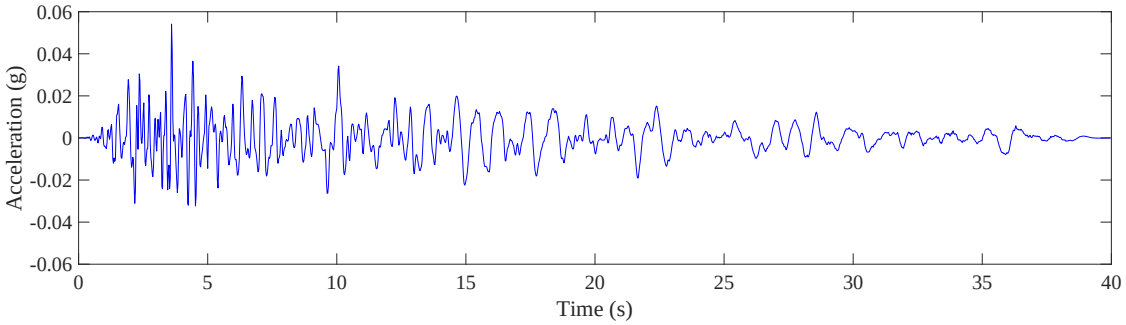

Figure 6. Input ground acceleration of the serviceability earthquake (Livermore earthquake, 1980).

3.1.2. Design Earthquake

The second input considered is the ground acceleration due to the design earthquake. The response of the structure with the isolator to this excitation becomes crucial for the design. Therefore, 15 artificially generated earthquakes obtained from the decomposition of the MCE defined in ASCE 7-16 [1] with different random phase angle for each frequency are used. All of them have a Peak Ground Acceleration (PGA) of 0.40 g, resulting in an intensity between VIII and IX and a magnitude around Mw = 7.

The ACELSIN© [25] software, which makes use of the methodology proposed by Gasparini and Vanmarcke [26], is used to obtain the time histories for each artificial earthquake. This methodology uses the decomposition of the spectrum shown by a black line in Figure 7a to generate fifteen accelerograms corresponding to the same seismic zone. Each time history (TH) is also integrated and superposed over the design spectrum in the same figure. The methodology also requires an intensity function (that is, a TH envelope), obtained from an earthquake, of similar magnitude and at the same location, to be applied to each of the generated THs. In this case, "El Centro Earthquake", which corresponds to the same seismic zone and magnitude of the MCE, is chosen to illustrate the methodology. A sequence with all of them is shown in Figure 8a. A zoom of the seventh event is plotted in Figure 8b. In order to check how these events fit the MCE, the spectra obtained from each individual TH are overlapped in Figure 7a. Finally, Figure 7b shows the all Fast Fourier Transforms (FFT) of each artificial earthquake event in order to show their frequency content.

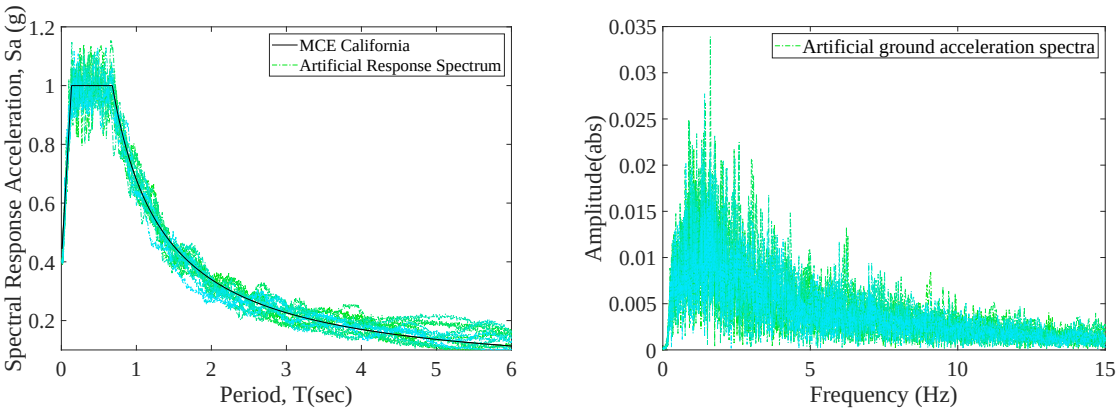

(**a**) Design response spectrum and response spectra

(**b**) FFT of the artificial earthquakes

Figure 7. Design response spectrum and Fast Fourier Transforms (FFT) of the input ground acceleration.

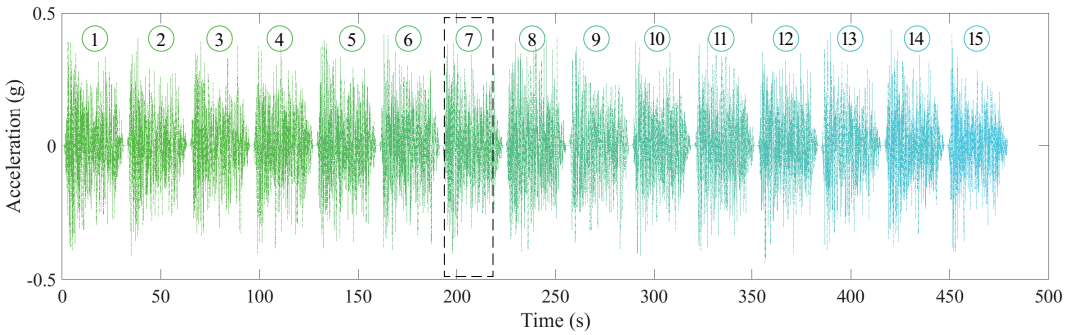

(**a**) Total input ground acceleration

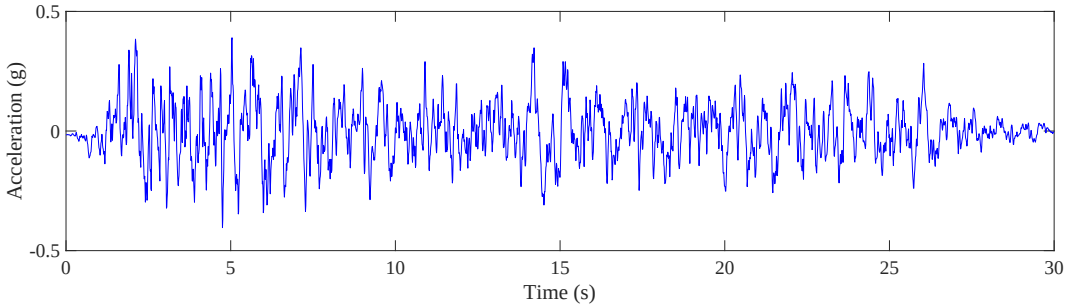

(**b**) Ground acceleration of the seventh event

Figure 8. Input ground acceleration of the design earthquake.

3.2. Performance Index

This section introduces the PIs used to evaluate the isolator performance and to define the performance function for the optimization problem . The PIs are the structure acceleration (J_1), the base displacement (bearing plate displacement) (J_2), the inter-story drift (J_3), and the mechanical energy (J_4). The subindexes P and RMS will indicate peak value and root mean square value, respectively, of the PIs. Additionally, the subindexes S and T will indicate the integral value of the mechanical energy only of the structure and of the total system (isolator + structure), respectively. Each PI is normalized to the response of the non-isolated structure identified by symbol " $\widehat{\ }$ ", thus, ($\ddot{\widehat{x}}_p$, $\widehat{x}_p$, $\widehat{E}_m$) are the acceleration, displacement, and mechanical energy of the non-isolated structure, respectively.

Different from the former magnitudes, the bearing displacement (x_a) is normalized to the minimum value of displacement capacity "d_1 "(see Figure 2a), obtained for the maximum frequency limit (that is, the minimum plate size) of the FPS within the optimization process. That is, J_2 will penalize greater sizes of the FPS. Hence, the definition of the PIs is a follows:

→ Normalized Peak Acceleration

$$J_{1,P} = \frac{max|\ddot{x}_p(t)|}{max|\ddot{\widehat{x}}_p(t)|},$$

→ Normalized RMS Acceleration

$$J_{1,RMS} = \frac{RMS(\ddot{x}_p(t))}{RMS(\ddot{\widehat{x}}_p(t))},$$

→ Normalized Bearing Displacement

$$J_{2,P} = \frac{max|x_a(t)|}{max|d_1(t)|},$$

→ Normalized RMS Bearing Displacement

$$J_{2,RMS} = \frac{RMS(x_a(t))}{RMS(d_1(t))},$$

→ Normalized Structure Drift

$$J_{3,P} = \frac{max|x_p(t) - x_a(t)|}{max|\widehat{x}_p(t)|},$$

→ Normalized RMS Structure Drift

$$J_{3,RMS} = \frac{RMS(x_p(t) - x_a(t))}{RMS(\widehat{x}_p(t))},$$

→ Normalized Mechanical Energy Structure

$$J_{4,S} = \frac{\int_0^t E_{m,S}(t)\,dt}{\int_0^t \widehat{E}_{m,S}(t)\,dt},$$

→ Normalized Mechanical Energy System

$$J_{4,T} = \frac{\int_0^t E_{m,T}(t)\,dt}{\int_0^t \widehat{E}_{m,S}(t)\,dt}.$$

3.3. Sensitivity Analysis

Previously to set the design process, a sensitivity analysis is carried out. Firstly, the single FPS (Figure 4a) is analyzed under the serviceability earthquake in order to study how the friction coefficient affects the FPS under low-intensity earthquakes. Thus, a value of μ will be chosen in order to avoid breakaway effects. Secondly, the FPS+VD and the phase-controlled FPS+SD are studied using the value of μ obtained in the first analysis. For the passive one, the viscous damping c_a with respect to the frequency of the pendulum f_a is studied. For the smart version, the unblocking damping (normal functioning) c_{min} with respect to f_a is analyzed (see Equation (9)).

Table 1 summaries the parameters adopted for the sensitivity analysis.

Table 1. Parameters for the sensitivity analysis.

Modal Parameters			
Structure		**Value**	
m_p	Mass	24,000	kg
f_p	Frequency	2.0	Hz
ζ_p	Damping ratio	1.0	%
c_p	Damping	6031.9	kg/s
k_p	Stiffness	3789.9×10^3	N/m
FPS+VD/FPS+SD		**Value**	
m_a	Mass	240	kg
f_a	Frequency	[0.50 to 1.10]	Hz
μ	Friction coefficient	[0.01 to 0.20]	%
c_a	Viscous damper	$[0.01c_p$ to $0.50c_p]$	kg/s
c_{min}	Semi-active damper	$[0.01c_p$ to $0.50c_p]$	kg/s
c_{max}	Semi-active damper	$10c_p$	kg/s

$J_{1,P}$ and $J_{2,P}$ are shown in Figure 9 for the single FPS under the serviceability earthquake. It can be observed that a low friction coefficient between 0.03–0.06 provides better performance under the low-intensity earthquake. In Figure 9a, the peak acceleration $J_{1,P}$ is shown, and values of $J_{1,P}$ between 0.32–0.53 can be achieved for all f_a values if $\mu \in (0.03, 0.06)$. If one pays attention to $J_{2,P}$ (Figure 9b) the peak isolator displacement, for $\mu < 0.03$, much higher isolator displacement is demanded. From Figure 9a, it can be observed that higher values of μ produces a stepwise degradation of the performance and will get the isolator involved in undesirable residual displacements leading to breakaway effects.

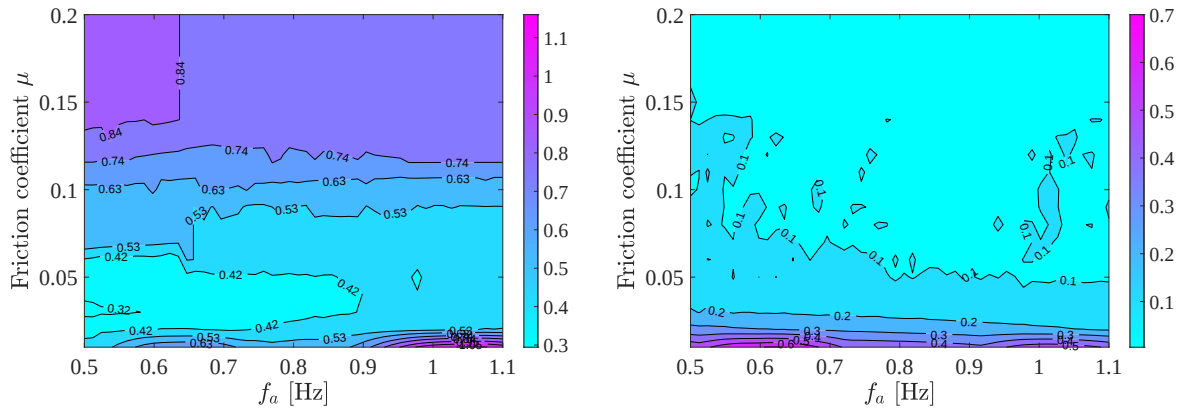

(**a**) $J_{1,P}$ (**b**) $J_{2,P}$

Figure 9. Sensitivity analyses. Response of the single FPS under the serviceability earthquake.

Now, the sensitivity analysis for the FPS+VD and for the phase-controlled FPS+SD are carried out using $\mu = 0.05$. Figures 10 and 11 show the contour plots of J_1 and J_3 for both cases. The values of J_1 are significantly smaller for the semi-active version. In both cases, from smaller plate sizes than a particular one, the isolated structure performance (Figure 10a,b) may be worse than the non-isolated one. However, the semi-active controlled version improves the performance for a broad range of plate sizes. From Figure 10b, it can be observed that the performance of the FPS+SD is almost constant from a minimum size of the FPS (maximum value of f_a). Hence, any f_a smaller than 0.85 Hz will provide the best performance. From the RMS values (Figure 10d), the isolator shows a performance that is almost independent of c_{min}. However, this fact does not happen with the passive version (Figure 10c). Additionally, the influence of f_a (the concave plate size) is quite low for a

semi-active case. Interestingly, the contour plots for J_3, the inter-story drift, show similar qualitative behavior to J_1. Again, the isolator will work from a particular size of the plate.

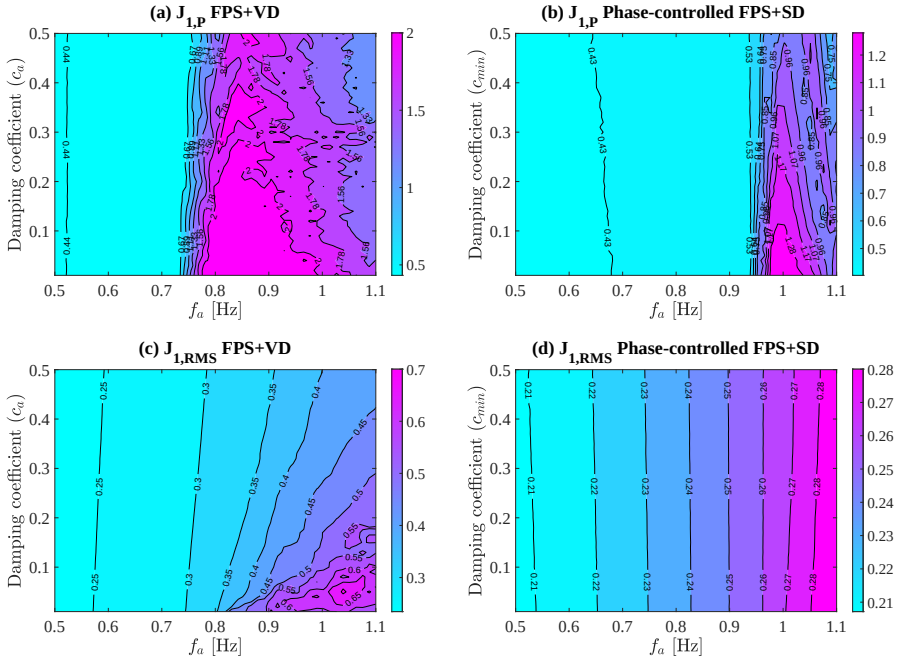

Figure 10. J_1 for FPS+VD and phase-controlled FPS+SD under the design earthquake.

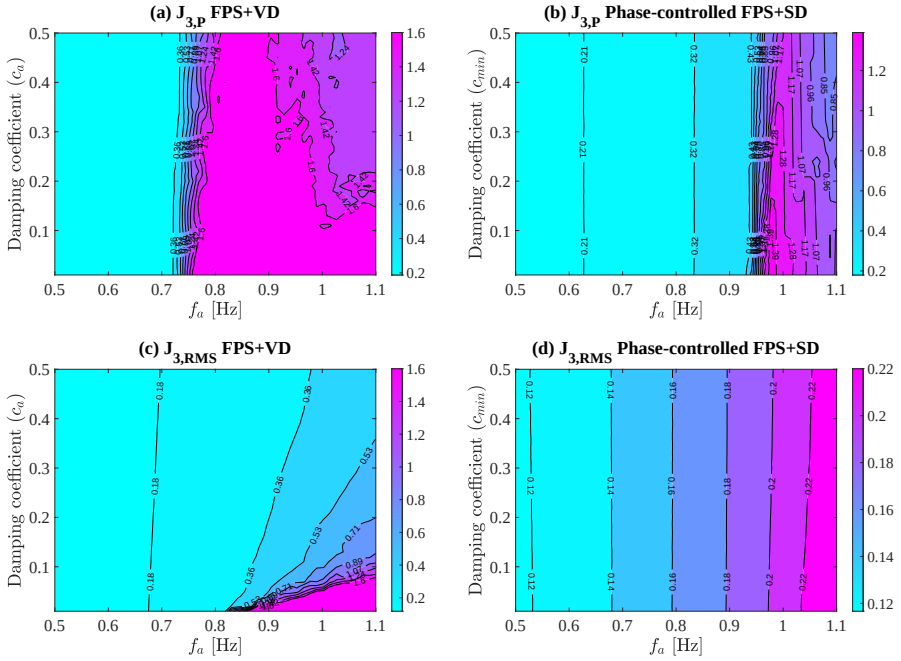

Figure 11. J_3 for FPS+VD and phase-controlled FPS+SD under the design earthquake.

Finally, it is worthy to mention that the contour plots obtained for phase-controlled and energy-controlled FPS+SD are quite similar. As an example and for comparison with Figure 11d, Figure 12 shows $J_{3,RMS}$ for the energy-controlled FPS+SD.

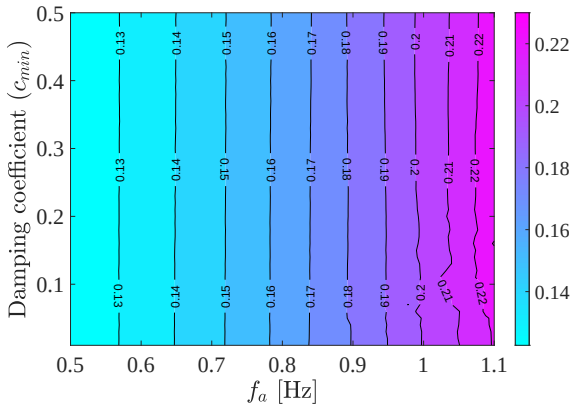

Figure 12. $J_{3,RMS}$ for energy-controlled FPS+SD under the design earthquake.

3.4. Optimization Problem

A two-step design process based on minimizing two performance functions ϕ_1 and ϕ_2 is proposed. The objective is to design, firstly the friction coefficient μ and secondly, the plate size (the pendulum natural frequency f_a) and the normal functioning damping coefficient c_a (for the passive version), or c_{min} (for the semi-active version). The first step consists of minimizing a performance function ϕ_1 and obtaining the optimum friction coefficient μ for the single FPS (without damper) under serviceability condition is such a way that good re-centering capacity is assured. In a second step, under the design earthquake, the frequency of the pendulum and the normal function damping coefficient are obtained by minimizing a performance function ϕ_2. Thus, the two-step design process is as follows:

- Step 1. Single FPS (Figure 4a) under the serviceability earthquake. The performance function ϕ_1 is defined as:

$$\phi_1(\underline{z}, \mu, f_a) = a_1 J_{1,P} + a_2 J_{2,P}, \tag{13}$$

in which $\underline{z} = [m_p, k_p, c_p, m_a]$, $a_1 = a_2 = 0.50$ are the weighting factors. The optimum value of μ for the range of f_a (plate sizes) considered is calculated from the:

$$\min_{\mu} \quad \phi_1(\underline{z}, \mu, f_a) \tag{14}$$

$$\text{suject to } f_a(\underline{z}) \in [f_{a,min}; f_{a,max}], \forall_\mu \in [\mu_{min}; \mu_{max}]. \tag{15}$$

- Step 2. FPS+VD or FPS+SD (Figure 4b,c) under the design earthquake. The performance function ϕ_2 is defined as:

$$\phi_2(\underline{z}, c_{min}, f_a) = \sum_{i=1}^{3} a_i J_{i,P} + \sum_{i=1}^{3} b_i J_{i,RMS}, \tag{16}$$

with $\sum_{i=1}^{3}(a_i + b_i) = 1$ and $\underline{z} = [m_p, k_p, c_p, m_a, \mu, c_{max}]$, where a_i and b_i are the weighting factors of control effects adjustment for a balance between the peak and RMS PIs, respectively. Generally speaking, ϕ_2 is a performance function that considers a balance between structural magnitudes (J_1 and J_3), acceleration and inter-story drift, and the plate displacement J_2, since this magnitude is normalized to the minimum plate size displacement. The minimization of ϕ_2 will reduce simultaneously, the structural magnitudes and the plate size. In this sense, the continuous movement of the bearing plate ($J_{2,RMS}$) should not be penalized ($b_2 = 0$), and however, the peak value of the plate displacement ($J_{2,P}$) should be penalized ($a_2 = 1/6$) in order to choose the minimum plate size that provides good performance (as it was shown in Figures 10 and 11).

Regarding the structure performance, ϕ_2 pays attention mainly to the peak of the inter-story drift $J_{3,P}$ ($a_3 = 1/3$) since this magnitude is crucial to avoid structural damages during the event. The remainder of the PIs, peak and RMS structure acceleration ($J_{1,P}$, and $J_{1,RMS}$) and the RMS of the inter-story drift are equally penalized (1/6) with a weight factor which is half of the peak of the inter-story drift. Thus, the optimum damping coefficient c_a for FPS+VD or c_{min} for FPS+SD (when the MR damper is normally functioning), and the pendulum natural frequency f_a(which defines the plate size) are calculated from the minimization of ϕ_2 as follows:

$$\min_{c_{min}, f_a} \quad \phi_2(\underline{z}, c_{min}, f_a), \tag{17}$$

$$\text{suject to } f_a(\underline{z}) \in [f_{a,min}; f_{a,max}], c_{min} \in [0; c_{max}]. \tag{18}$$

Note that $c_{min} = c_a$ in Equation (17) if the FPS+VD is being designed. Note also that the proposed design process requires two sequential inputs, first, a low-intensity earthquake followed by a design earthquake corresponding to the considered seismic area. The selection of the design earthquake according to current codes has been explained in Section 3.1.

4. Example of Design

The optimization process for the design of the isolated-structure is now applied to the structure described in Table 1. The isolator parameters considered for the optimization are also presented in the table. The optimization process has been run for three cases: (i) FPS+VD in which the optimization parameters are, f_a and c_a, (ii) FPS+SD with phase control and (iii) FPS+SD with energy-predictive-based control. The optimization parameters for the last two cases are f_a and c_{min} (which corresponds to a damping ratio ζ_{min}).

From Step 1 of the optimization problem, a friction coefficient of $\mu = 0.05$ has been obtained. Note that this value is the same for three cases. Thus, Table 2 collects the configuration parameters once Step 2 is run and the minimum values of the performance function (ϕ_2) (Equation (17)) together with its reduction with respect to the non-isolated structure. Furthermore, for comparison reasons, two more cases are included in this table, the optimum single FPS using $\mu = 0.05$ (low-friction FPS) and $\mu = 0.20$ (high-friction FPS), which correspond to the optimum friction coefficients for the serviceability and design earthquake, respectively. Note that, when a single FPS is subjected to the design earthquake, the optimum performance function is achieved for the maximum possible friction coefficient μ_{max} ($\mu = 0.20$) used within the optimization problem (see Table 1).

Table 3 summarizes the results obtained for all the PIs. The PI based on the mechanical energy, $J_{4,S}$ and $J_{4,T}$ are also presented in the table.

Table 2. Optimum parameters for the isolator configurations studied.

System	f_a	μ	$\zeta_{(c_a, c_{min})}$	ϕ_2	Reduction (%)
Non-isolated structure	-	-	-	0.833	0.00
$FPS_{\mu=0.05}$	0.671	0.05	-	0.834	0.00
FPS+VD	0.647	0.05	0.500	0.791	5.04
FPS+SD (Phase control)	0.684	0.05	0.480	0.564	32.29
FPS+SD (Energy control)	0.745	0.05	0.240	0.571	31.45
$FPS_{\mu=0.20}$	0.671	0.20	-	0.529	36.49

Table 3. Performance indexes (PIs) for the optimum configurations under the design earthquake.

System	$J_{1,P}$	$J_{1,RMS}$	$J_{2,P}$	$J_{2,RMS}$	$J_{3,P}$	$J_{3,RMS}$	$J_{4,S}$	$J_{4,T}$
Non-isolated structure	1.000	1.000	-	-	1.000	1.000	1.000	1.000
$FPS_{\mu=0.05}$	0.522	0.446	3.111	0.975	0.313	0.297	0.848	0.178
FPS+VD	0.478	0.419	3.015	0.886	0.286	0.263	0.692	0.141
FPS+SD (Phase control)	0.434	0.359	1.891	0.469	0.239	0.225	0.209	0.052
FPS+SD (Energy control)	0.473	0.385	1.778	0.413	0.273	0.245	0.173	0.051
$FPS_{\mu=0.20}$	0.476	0.408	1.420	0.257	0.274	0.321	0.081	0.033

From Tables 2 and 3, it can be observed that both semi-active designs behave better than the FPS+VD and much better than the FPS with $\mu = 0.05$. To achieve similar results as to the semi-active version with the single FPS, much higher values of μ are needed, and consequently, the behavior under lower intensity earthquakes will be drastically affected. Paying attention to $J_{3,P}$, which is the main PI considered within the performance function, the phase-controlled FPS+SD shows the best performance, achieving a reduction of 76%.

The cumulative distribution function (CDF) curves for the bearing plate displacement and for the inter-story drift using the optimum configurations of Table 2 under the design earthquake (Figure 13) and the serviceability earthquake (Figure 14) are computed and plotted. The CDFs indicate the percentage of time of non-exceedance of a value of the considered magnitude.

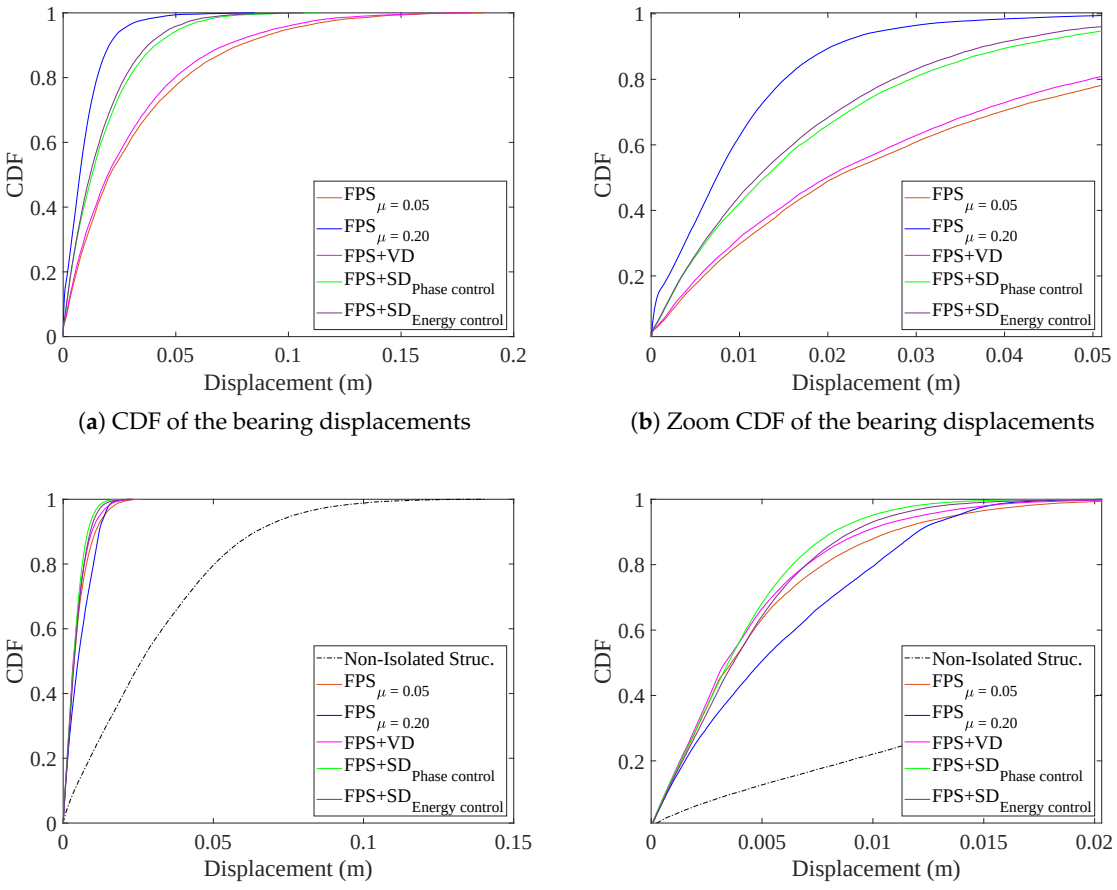

(**a**) CDF of the bearing displacements

(**b**) Zoom CDF of the bearing displacements

(**c**) CDF of the drift response of the structure

(**d**) Zoom to CDF of the drift response of the structure

Figure 13. Cumulative distribution function (CDF) of bearing plate displacement and drift under the design earthquake.

Figure 13a,b show that the FPS with high friction exhibits much minor bearing plate displacements in comparison with the FPS+VD, both semi-active versions, and the FPS with low friction. The FPS+VD and FPS with low friction show more displacement. FPS+SD with phase control and energy-predictive-based control have similar behavior and present minor displacement than the FPS+VD. From Figure 13c,d, it can be observed that the FPS+VD presents more capacity to control the drift than the single FPS and similarly, the semi-active versions show better performance than the FPS+VD. Finally, the phase-controlled FPS+SD always behaves slightly better than the energy-predictive-based one.

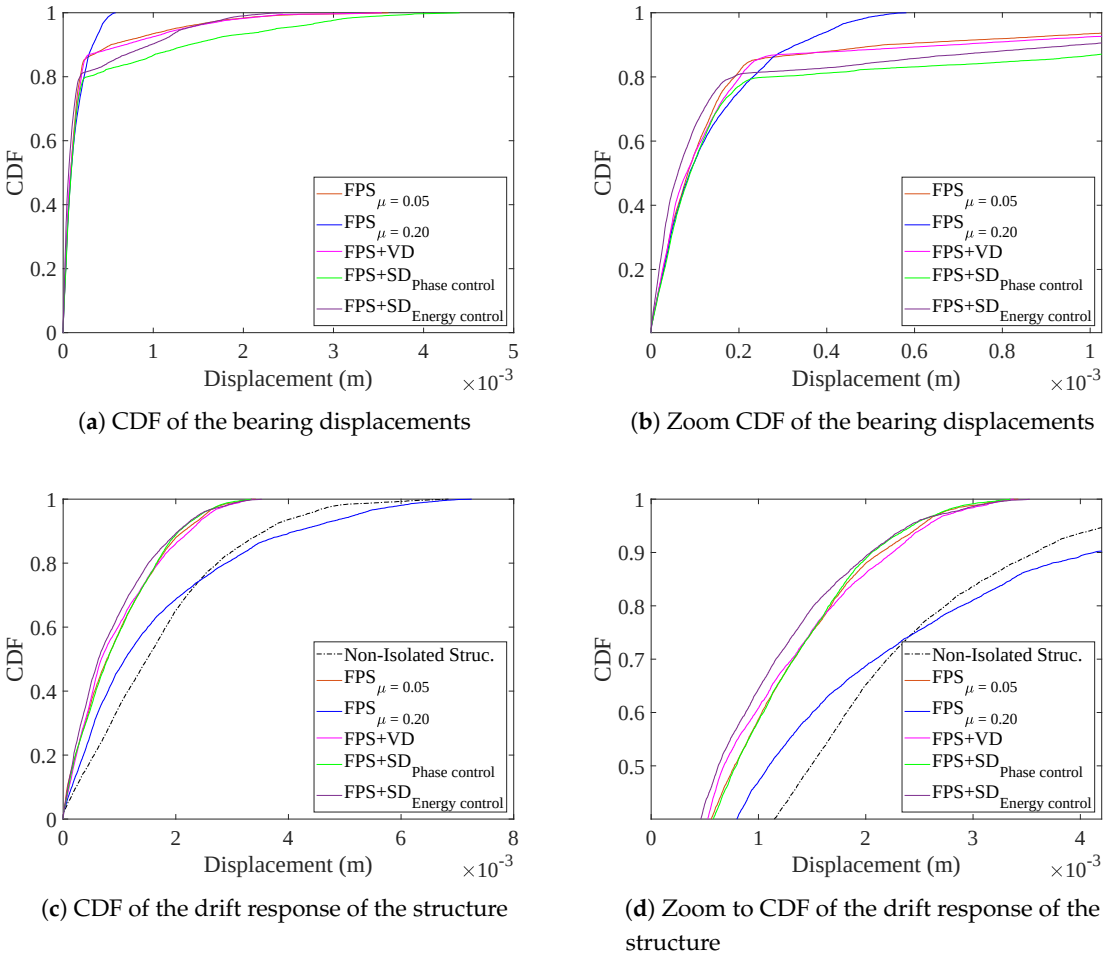

(**a**) CDF of the bearing displacements

(**b**) Zoom CDF of the bearing displacements

(**c**) CDF of the drift response of the structure

(**d**) Zoom to CDF of the drift response of the structure

Figure 14. CDF of bearing plate displacement and drift under the serviceability earthquake.

Figure 14 shows the same plots as those of Figure 13 but for the serviceability earthquake. Now, it is clearly appreciated that all the low-friction FPSs show similar performance in terms of the drift. The high friction FPS is unable to filter out low-intensity earthquakes.

5. Results and Analysis

5.1. Performance under Several Earthquakes

The isolator configurations studied in the former section (Table 2) are now numerically tested under eight selected earthquakes. As an example, the input ground acceleration, the structure acceleration, the bearing plate displacement and the inter-story drift responses for one of the earthquakes, the Northridge earthquake (17 January 1999, magnitude of 6.7 Mw) are plotted in Figure 15. All configurations are effectively working for the range of maximum ground acceleration.

When the earthquake intensity is reduced, the high-friction-coefficient FPS tends to behave as the non-isolated structure, that is, it is unable to filter out the input ground motion. Moreover, it can be observed that both semi-active strategies perform in a similar way. Indeed, the CDFs for the bearing plate displacement and the inter-story drift are computed in Figure 16. Similar conclusions as for Figure 15 can be stated from this figure.

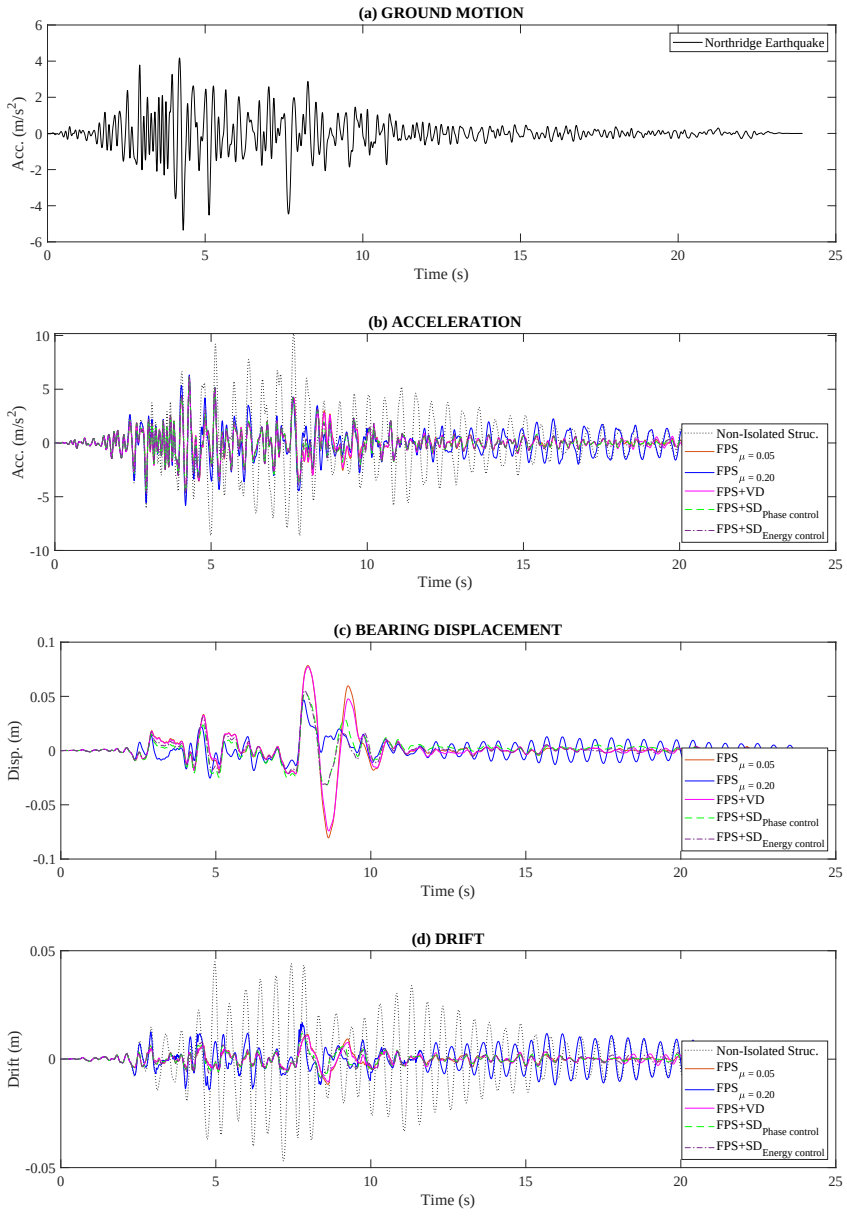

Figure 15. Time history (TH) to Northridge earthquake for the five isolator configurations studied.

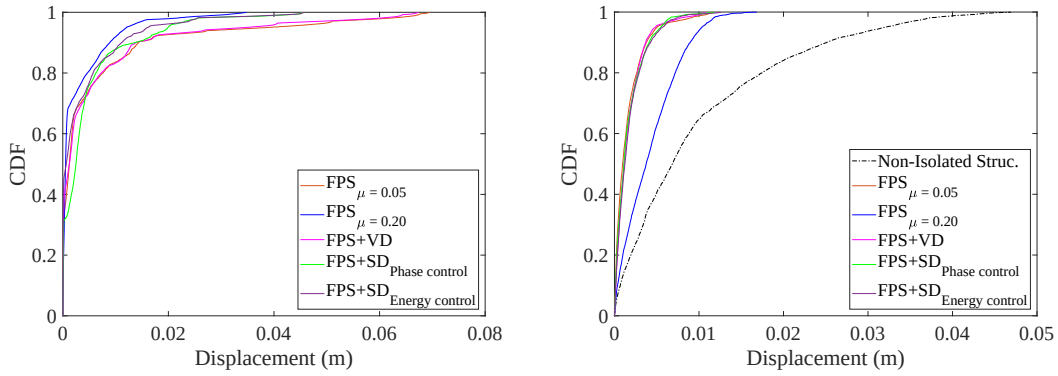

(**a**) CDF curves of the bearing displacements

(**b**) CDF curves of the inter-story drift

Figure 16. CDF curves under the Northridge earthquake.

Table 4 shows the PIs achieved for the eight selected earthquakes. They are located in the USA (North American plate), Japan (Pacific plate), New Zealand (Indo-Australian plate), and finally Italy and Greece (Eurasian plate) [27]. An important point to highlight is that the influence of the TH record and the frequency content in earthquakes, with similar intensity, may change drastically the system response. As an example, if one compares Corinth and Imperial Valley events, the last one is shorter, with broader frequency content, lower PGA, and high RMS value than the first one. The results of this table are summarized in terms of the performance function ϕ_2 in Figure 17.

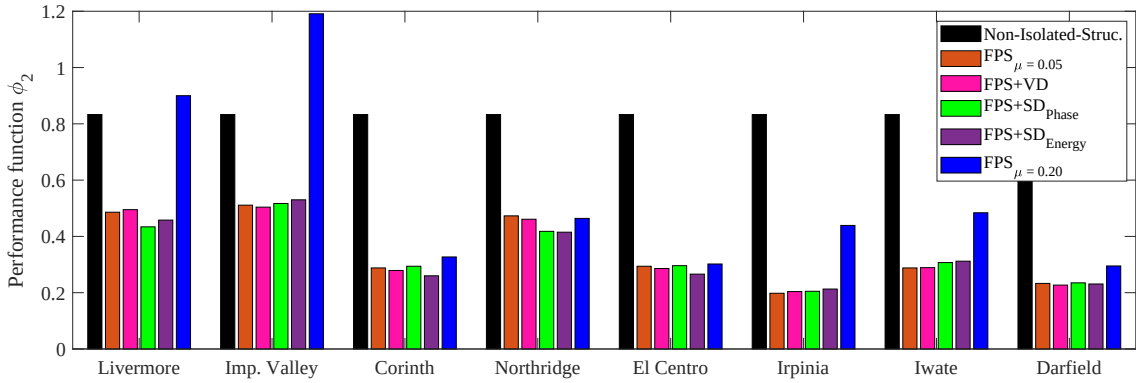

Figure 17. Performance function ϕ_2 of the configurations studied for the eight earthquakes.

5.2. Performance Discussion

The performance of the different configurations is further studied hereof. Firstly, the performance for a range of concave plate radii is studied. Secondly, the performance for the same concave plate is analyzed, and finally, the robustness of the isolator configurations under variation of the friction coefficient μ is studied.

Table 4. Response under selected earthquakes.

Earthquake	System	$J_{1,P}$	$J_{1,RMS}$	$J_{2,P}$	$J_{2,RMS}$	$J_{3,P}$	$J_{3,RMS}$	$J_{4,S}$	$J_{4,T}$	ϕ_2
Livermore 5.8 Mw USA	Non-isolated	1.000	1.000	-	-	1.000	1.000	1.000	1.000	0.833
	$FPS_{\mu=0.05}$	0.760	0.554	0.071	0.013	0.492	0.544	0.408	0.318	0.486
	FPS+VD	0.776	0.580	0.056	0.009	0.495	0.566	0.395	0.336	0.495
	$FPS+SD_{Phase}$	0.648	0.433	0.078	0.018	0.482	0.455	0.369	0.233	0.434
	$FPS+SD_{Energy}$	0.655	0.547	0.050	0.008	0.482	0.532	0.345	0.297	0.458
	$FPS_{\mu=0.20}$	1.133	1.072	0.010	0.003	1.059	1.068	1.287	1.190	0.900
Imp. Valley 6.5 Mw USA	Non-isolated	1.000	1.000	-	-	1.000	1.000	1.000	1.000	0.833
	$FPS_{\mu=0.05}$	0.864	0.763	0.069	0.019	0.441	0.486	0.418	0.310	0.511
	FPS+VD	0.868	0.760	0.052	0.017	0.432	0.479	0.390	0.298	0.504
	$FPS+SD_{Phase}$	0.897	0.761	0.069	0.023	0.460	0.453	0.426	0.285	0.517
	$FPS+SD_{Energy}$	0.855	0.773	0.065	0.016	0.487	0.515	0.415	0.330	0.530
	$FPS_{\mu=0.20}$	0.953	1.288	0.110	0.011	1.656	1.484	2.459	2.255	1.191
Corinth 6.6 Mw GREECE	Non-isolated	1.000	1.000	-	-	1.000	1.000	1.000	1.000	0.833
	$FPS_{\mu=0.05}$	0.352	0.177	0.793	0.114	0.140	0.123	0.166	0.049	0.288
	FPS+VD	0.346	0.176	0.766	0.113	0.132	0.123	0.160	0.046	0.279
	$FPS+SD_{Phase}$	0.345	0.178	0.820	0.114	0.148	0.127	0.158	0.046	0.294
	$FPS+SD_{Energy}$	0.303	0.185	0.618	0.087	0.157	0.140	0.113	0.044	0.260
	$FPS_{\mu=0.20}$	0.332	0.267	0.597	0.067	0.258	0.248	0.124	0.077	0.327
Northridge 6.69 Mw USA	Non-isolated	1.000	1.000	-	-	1.000	1.000	1.000	1.000	0.833
	$FPS_{\mu=0.05}$	0.597	0.407	1.156	0.239	0.248	0.181	0.766	0.202	0.473
	FPS+VD	0.596	0.405	1.126	0.227	0.231	0.176	0.684	0.180	0.461
	$FPS+SD_{Phase}$	0.588	0.392	0.863	0.152	0.245	0.176	0.340	0.116	0.418
	$FPS+SD_{Energy}$	0.602	0.408	0.759	0.133	0.268	0.185	0.294	0.115	0.415
	$FPS_{\mu=0.20}$	0.607	0.514	0.581	0.098	0.357	0.370	0.274	0.180	0.464
El Centro 6.9 Mw USA	Non-isolated	1.000	1.000	-	-	1.000	1.000	1.000	1.000	0.833
	$FPS_{\mu=0.05}$	0.338	0.221	0.827	0.190	0.125	0.126	0.234	0.065	0.294
	FPS+VD	0.333	0.221	0.803	0.190	0.117	0.125	0.230	0.062	0.286
	$FPS+SD_{Phase}$	0.344	0.220	0.824	0.175	0.129	0.132	0.197	0.057	0.296
	$FPS+SD_{Energy}$	0.312	0.227	0.617	0.143	0.145	0.147	0.155	0.057	0.266
	$FPS_{\mu=0.20}$	0.392	0.279	0.465	0.090	0.218	0.240	0.116	0.073	0.302
Irpinia 6.9 Mw ITALY	Non-isolated	1.000	1.000	-	-	1.000	1.000	1.000	1.000	0.833
	$FPS_{\mu=0.05}$	0.231	0.204	0.239	0.049	0.161	0.189	0.131	0.054	0.198
	FPS+VD	0.243	0.213	0.251	0.049	0.159	0.199	0.132	0.057	0.204
	$FPS+SD_{Phase}$	0.242	0.218	0.241	0.047	0.163	0.205	0.124	0.057	0.205
	$FPS+SD_{Energy}$	0.261	0.230	0.206	0.038	0.182	0.219	0.107	0.059	0.213
	$FPS_{\mu=0.20}$	0.510	0.511	0.200	0.030	0.455	0.502	0.315	0.268	0.439
Iwate 6.9 Mw JAPAN	Non-isolated	1.000	1.000	-	-	1.000	1.000	1.000	1.000	0.833
	$FPS_{\mu=0.05}$	0.523	0.360	0.279	0.056	0.164	0.239	0.289	0.0974	0.288
	FPS+VD	0.522	0.362	0.286	0.057	0.161	0.240	0.301	0.098	0.289
	$FPS+SD_{Phase}$	0.554	0.373	0.294	0.056	0.183	0.255	0.292	0.105	0.307
	$FPS+SD_{Energy}$	0.577	0.383	0.239	0.043	0.199	0.276	0.223	0.105	0.312
	$FPS_{\mu=0.20}$	0.735	0.561	0.218	0.026	0.438	0.516	0.345	0.281	0.484
Darfield 7.0 Mw NEW ZEALAND	Non-isolated	1.000	1.000	-	-	1.000	1.000	1.000	1.000	0.833
	$FPS_{\mu=0.05}$	0.488	0.227	0.438	0.047	0.080	0.084	0.043	0.018	0.233
	FPS+VD	0.484	0.229	0.411	0.047	0.076	0.087	0.044	0.019	0.227
	$FPS+SD_{Phase}$	0.491	0.233	0.421	0.047	0.088	0.090	0.043	0.019	0.235
	$FPS+SD_{Energy}$	0.512	0.237	0.324	0.037	0.109	0.095	0.035	0.019	0.231
	$FPS_{\mu=0.20}$	0.579	0.303	0.312	0.027	0.186	0.201	0.062	0.051	0.295

Figure 18 shows the performance function ϕ_2 and the normalized structure mechanical energy $J_{4,S}$ for the serviceability earthquake and for the design earthquake, considering a range of concave plate radii (in consonance with the minimum and maximum value of the pendulum natural frequency f_a). It can be concluded that the semi-active damper of the FPS acts when needed, avoiding

stroke saturation under large ground motions, and showing low friction performance under low ground motions. From Figure 18a,b, it can be observed that the high-friction FPS cannot cope with low ground motions. From Figure 18c,d, it can be observed that small plate sizes for the semi-active versions can also be really effective. Additionally, for the low-friction single FPS and the FPS+VD, for small plate sizes, the performance is even worse than the one of the non-isolated structure.

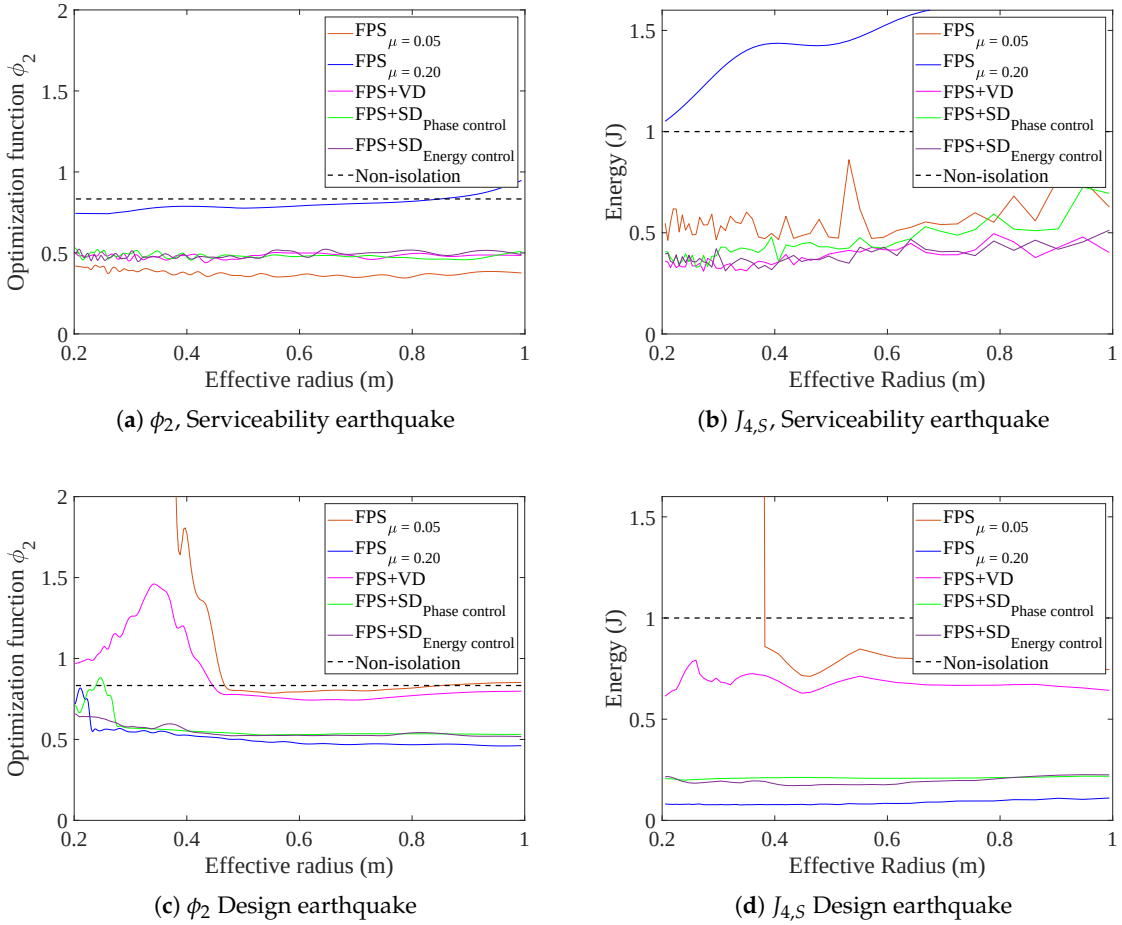

(**a**) ϕ_2, Serviceability earthquake

(**b**) $J_{4,S}$, Serviceability earthquake

(**c**) ϕ_2 Design earthquake

(**d**) $J_{4,S}$ Design earthquake

Figure 18. Performance function ϕ_2 and structure energy for a range of effective FPS radii.

Table 5 summarizes the optimization function values and the improvement obtained for each isolation system with the same concave plate size (R_{eff}) under the serviceability and design earthquake. The semi-active isolators are effective for both earthquakes while the FPS+VD and the low-friction FPS are only effective for the serviceability earthquake and the high-friction FPS only works for the design earthquake.

The performance function ϕ_2 for the configuration studied is plotted for the range of the friction coefficient μ used for the optimization problem (see Figure 19). Clearly, it is observed that the single FPS needs a low friction coefficient ($\leq$0.07) in order to cope with the serviceability earthquake. On the other way around, the FPS needs a high friction coefficient ($\geq$0.17) to be able to dissipate the energy demand of the design earthquake. The passive FPS and the semi-active ones are robust to changes in the friction coefficient, and the semi-active versions are working effectively for both earthquakes.

Table 5. Summary of the results for the same effective radius size.

Serviceability Earthquake						
System	R_{eff}	f_a	μ	$\zeta_{(c_a,c_{min})}$	ϕ_2	**Reduction (%)**
$FPS_{\mu=0.05}$	0.300	0.867	0.05	-	0.491	50.90
FPS+VD	0.300	0.867	0.05	0.500	0.504	49.60
FPS+SD (Phase control)	0.300	0.867	0.05	0.480	0.480	52.00
FPS+SD (Energy control)	0.300	0.867	0.05	0.240	0.470	53.00
$FPS_{\mu=0.20}$	0.300	0.867	0.20	-	0.930	7.00
Design Earthquake						
System	R_{eff}	f_a	μ	$\zeta_{(c_a,c_{min})}$	ϕ_2	**Reduction (%)**
$FPS_{\mu=0.05}$	0.300	0.867	0.05	-	5.614	0.00
FPS+VD	0.300	0.867	0.05	0.500	1.476	0.00
FPS+SD (Phase control)	0.300	0.867	0.05	0.480	0.608	39.20
FPS+SD (Energy control)	0.300	0.867	0.05	0.240	0.612	38.80
$FPS_{\mu=0.20}$	0.300	0.867	0.20	-	0.599	40.10

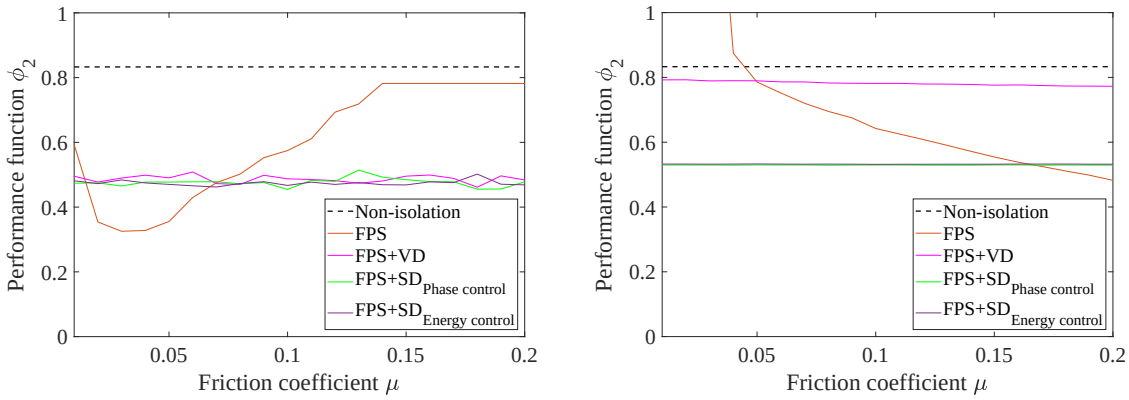

(**a**) ϕ_2 under serviceability earthquake (**b**) ϕ_2 under design earthquake

Figure 19. Performance function ϕ_2 and structure energy for a range of effective FPS radii.

6. Concluding Remarks

This paper works on the design of FPS isolators with a damper that can be passive or semi-active. That is, two types of isolation systems have been considered and studied: (i) an FPS together with a passive damper (FPS+VD), and (ii) an FPS with a smart damper, (FPS+SD). For this configuration, two ON-OFF control laws have been studied. The first one is a simple collocated phase control and the second one is a model-based control law that uses an energy-predictive algorithm to decide the state of the ON-OFF control.

A design methodology focused on FPSs with an additional damper has been proposed. The methodology is based on a two-step design process that accounts for low and high-intensity earthquakes. Each step is based on a performance function that weights different performance indexes in terms of their peak and RMS values. More concretely, the following remarks can be extracted:

- The FPS with low friction exhibits large bearing displacements under the design earthquake, while the FPS with high friction is not able to cope with the bearing displacement demand under the serviceability earthquake, producing undesirable residual displacements when the earthquake ends.
- The implementation of an FPS+VD allows us to use a concave plate with low friction, increasing thus the re-centering capacity and avoiding the residual displacements.

- The FPS+SD controls the bearing plate displacement acting when needed: avoiding stroke saturation under large ground motions and showing a very low friction FPS under serviceability ground motions. Additionally, for a similar performance as compared to a single FPS or the FPS+VD, the plate size for the FPS+SD may be significantly smaller.
- The single FPS performance depends importantly on the friction coefficient value; however, the FPS equipped with a damper is robust to changes of the friction coefficients, showing better performance when the damper is semi-active.
- The FPS+SD has similar behavior with a phase control and an energy-predictive-based control. However, the implementation of phase control in practice could be easily implementable as compared to energy control. The phase control requires to measure the response in acceleration and this is possible using directly an accelerometer in the concave plate. The energy-predictive-based control requires measuring the velocity and displacement of the structure and, this process could take a longer time for multi-story buildings. Additionally, an accurate model is needed to get this law to be effective.
- All studied configurations have been testing for the eight selected earthquakes and the FPS+SD has a robust and effective performance under earthquakes differently located.

Future works will focus on the following issues, which are geared to the practical application of the methodology proposed in this paper. The authors are working on the implementation of the proposed isolation strategy on the building presented in Shook et al. [28]. Thus, several issues have to be addressed: (i) the extension of the isolation strategy to bidirectional semi-active controlled FPS, (ii) the inclusion of a hysteretic model for the MR damper, (iii) the inclusion of a velocity-dependent friction model, (iv) a robustness analysis of the isolator performance under system uncertainties, such as vertical load variability, working temperature and time-varying friction coefficients, and (v) the inclusion of practical elements to get the phase control more effective, such as low-filtering of the ground motion.

Author Contributions: Conceptualization, C.A.B.-V. and I.M.D.; methodology, I.M.D.; software, C.A.B.-V. and J.M.S.; validation, I.M.D. and J.H.G.-P.; formal analysis, J.M.S. and J.H.G.-P.; investigation, C.A.B.-V. and I.M.D.; data curation, I.M.D. and J.H.G.-P.; writing—original draft preparation, C.A.B.-V.; writing—review and editing, I.M.D. All authors have read and agreed to the published version of the manuscript.

Funding: This research was funded by Ministry of Science, Innovation and Universities grant number RTI2018-099639-B-I00.

Conflicts of Interest: The authors declare no conflict of interest.

References

1. ACSE. *Minimum Design Loads and Associated Criteria for Buildings and Other Structures*; The American Society of Civil Engineers: Reston,VA, USA, 2017.
2. Akiyama, H. *Earthquake-Resistant Design Method for Buildings Based on Energy Balance*; Reverté, S.A.: Tokyo, Japan, 2002.
3. Aguiar, R.; Vergara, F.; Monge, J.P. Análisis Sísmico de una Estructura con Aisladores FPS de Primera y Segunda Generación y Elastoméricos Con Núcleo De Plomo. *Rev. Int. Ing. Estructuras* **2014**, *19*, 35–89.
4. Ponzo, F.; Di Cesare, A.; Leccese, G.; Nigro, D. Standard Requirements for the Recentring Capability of Curved Surface Sliders. *Ing. Sismica* **2019**, 3, 3323–3332.
5. Fenz, D.; Constantinou, M. Spherical Sliding Isolation Bearings with Adaptive Behavior: Theory. *Earthq. Eng. Struct. Dyn.* **2008**, *37*, 163–183. [CrossRef]
6. Weber, F.; Distl, J.; Braun, C. Isolation Performance Assessment of Adaptive Behaviour of Triple Friction Pendulum. *J. Civ. Eng. Res.* **2017**, *7*, 17–33.
7. Quaglini, V.; Gandelli, E.; Dubini, P. Numerical Investigation of Curved Surface Sliders under Bidirectional Orbits. *Ing. Sismica* **2019**, *2*, 1–19.

8. Aguiar, R.; Morales, E.; Guaygua, B.; Rodríguez, M. Método Simplificado para el Análisis Sísmico de Estructuras con Aisladores FPS de Tercera Generación. *Rev. Int. Metod. Numer. Para Calc. Diseño Ing.* **2017**, *33*, 103–109. [CrossRef]
9. Ponzo, F.; Di Cesare, A.; Leccese, G.; Nigro, D. Shake Table Testing on Restoring Capability of Double Concave Friction Pendulum Seismic Isolation Systems: Restoring Capability of Friction. *Earthq. Eng. Struct. Dyn.* **2017**, *46*, 2337–2353. [CrossRef]
10. Weber, F.; Distl, H.; Braun, C. Isolation Performance of Optimized Triple Friction Pendulum. *Int. Ref. J. Eng. Sci.* **2016**, *5*, 55–69.
11. Domenico, D.; Gandeli, E.; Quanglini, V. Adaptive Isolation System Combining Low-friction Sliding Pendulum Bearings and SMA-Based Gap Dampers. *Eng. Struct.* **2020**, *212*, 110536. [CrossRef]
12. Spencer, B., Jr.; Dyke, S.; Deoskar, H. Benchmark Problems in Structural Control: Part I—Active Mass Driver System. *Earthq. Eng. Struct. Dyn.* **1998**, *27*, 1127–1139. [CrossRef]
13. Chang, M.C.; Spencer, B., Jr. Active Base Isolation of Buildings Subjected to Seismic Excitations. *Earthq. Eng. Struct. Dyn.* **2010**, *39*, 1493–1512. [CrossRef]
14. Johnson, E.; Ramallo, J.C.; Spencer, B.; Sain, M. Intelligent Base Isolation Systems. In Proceedings of the Second World Conference on Structural Control, Kyoto, Japan, 28 June–1 July 1998; pp. 1–10.
15. Xu, Y.; Li, B. Hybrid Platform for High-Tech Equipment Protection against Earthquake and Microvibration. *Earthq. Eng. Struct. Dyn.* **2006**, *35*, 943–967. [CrossRef]
16. Kim, H.; Roschke, P. Design of Fuzzy Logic Controller for Smart Base Isolation System using Genetic Algorithm. *Eng. Struct.* **2006**, *28*, 84–96. [CrossRef]
17. Koo, J.H.; Ahmadian, M.; Setareh, M.; Murray, T.M. In Search of Suitable Control Methods for Semi-Active Tuned Vibration Absorbers. *J. Vib. Control* **2004**, *10*, 163–174. [CrossRef]
18. Weber, F.; Distl, H.; Braun, C. Semi-Active Base Isolation of Civil Engineering Structures Based on Optimal Viscous Damping and Zero Dynamic Stiffness. *Conf. Proc. Soc. Exp. Mech. Ser.* **2017**, *2*, 1–9.
19. Zhang, D.; Pan, P.; Zeng, Y.; Guo, Y. A Novel Robust Optimum Control Algorithm and Its Application to Semi Active Controlled Base Isolated Structures. *Bull. Earthq. Eng.* **2020**, *18*, 2431–2460. [CrossRef]
20. Gu, X.; Yu, Y.; Li, Y.; Li, J.; Askari, M.; Samali, B. Experimental Study of Semi-Active Magnetorheological Elastomer Base Isolation System using Optimal Neuro Fuzzy Logic Control. *Mech. Syst. Signal Process.* **2019**, *119*, 380–398. [CrossRef]
21. Spencer, B., Jr.; Yang, G.; Carlson, J.D.; Sain, M. "Smart" Dampers for Seismic Protection of Structures: A Full-Scale Study. In Proceedings of the Second World Conference on Structural Control, Kyoto, Japan, 28 June–1 July 1998.
22. Fu, W.; Zhang, C.; Sun, L.; Askari, M.; Samali, B.; Chung, K.; Sharafi, P. Experimental Investigation of a Base Isolation System Incorporating MR Dampers with the High-Order Single Step Control Algorithm. *Appl. Sci.* **2017**, *7*, 344. [CrossRef]
23. Preumont, S.; Seto, K. *Active Control of Structures*; John Wiley & Sons, Ltd.: Hoboken, NJ, USA, 2008.
24. Zelleke, D.; Matsagar, V. Energy-Based Predictive Algorithm for Semi-Active Tuned Mass Dampers. *Struct. Des. Tall Spec. Build.* **2019**, *12*, 1–20. [CrossRef]
25. Agudelo, J.A. ACELSIN©. Available online: https://estructurando.net/descargas/software/ (accessed on 8 February 2020).
26. Gasparini, D.; Vanmarcke, E. *Simulated Earthquake Motions Compatible with Prescribed Responde Spectra*; Department of Civil Engineering, Massachussets Institute of Technology: Cambridge, MA, USA, 1976.
27. PEER. The Web-Based Pacific Earthquake Engineering Research Center. Available online: https://https://ngawest2.berkeley.edu (accessed on 8 July 2020).
28. Shook, D.; Lin, P.; Lin, T.; Roschke, P. A Comparative Study in the Semi-Active Control of Isolated Structures. *Smart Mater. Struct.* **2007**, *16*, 1433. [CrossRef]